A System Level Energy Model and Energy-Quality Evaluation for Integrated Transceiver Front-Ends

Ye Li, Bertan Bakkaloglu, *Member, IEEE*, and Chaitali Chakrabarti, *Senior Member, IEEE*

***Abstract*—As CMOS technology scales down, digital supply voltage and digital power consumption goes down. However, the supply voltage and power consumption of the RF front-end and analog sections do not scale in a similar fashion. In fact, in many state-of-the-art communication transceivers, RF and analog sections can consume more energy compared to the digital part. In this paper, first, a system level energy model for all the components in the RF and analog front-end is presented. Next, the RF and analog front-end energy consumption and communication quality of three representative systems are analyzed: a single user point-to-point wireless data communication system, a multi-user code division multiple access (CDMA)-based system and a receive-only video distribution system. For the single user system, the effect of occupied signal bandwidth, peak-to-average ratio (PAR), symbol rate, constellation size, and pulse-shaping filter roll-off factor is analyzed; for the CDMA-based multi-user system, the effect of the number of users in the cell and multiple access interference (MAI) along with the PAR and filter roll-off factor is studied; for the receive-only system, the effect of $1/f$ noise for direct-conversion receiver and the effect of IF frequency for low-IF architecture on the RF front-end power consumption is analyzed. For a given communication quality specification, it is shown that the energy consumption of a wireless communication front-end can be scaled down by adjusting parameters such as the pulse shaping filter roll-off factor, constellation size, symbol rate, number of users in the cell, and signal center frequency.**

***Index Terms*—Energy-efficient, energy model, peak-to-mean ratio (PAR), pulse shaping roll-off factor, RF front-end.**

I. Introduction

WIRELESS communication and mobile computing devices are widely used in everyday life. All of these devices are powered by batteries with a limited lifetime. Since the advances in battery technology have failed to keep up with increasing current consumption in mobile communication devices, aggressive techniques to reduce the power consumption of wireless communication devices have to be developed.

Different aspects of low power wireless communication transceivers have been addressed in recent years. These include energy efficient modulation scaling [1], [2], [15], delay controlled transmission schemes [3]–[5], energy efficient routing [6]–[8], power management-based task scheduling for digital communication processors [9], etc. In most of the prior work, the power consumed in RF and analog sections are either ignored or represented by constant values. This may lead to erroneous energy evaluations since the RF and analog sections process analog signals with high frequency content and typically consume more energy compared to the digital part. For example, as shown in [10], an IEEE 802.11-b wireless LAN card based on Intersil's PRISM II chipset consumes about 110 mW for the medium access control (MAC) processor, 170 mW for the digital baseband electronics, 240 mW for the analog electronics, and 600 mW for the power amplifier. Since about 75% of the power is consumed in the analog and RF sections, it is important to develop an accurate and comprehensive energy model for these sections. Such a model would clearly help in developing a thorough tradeoff analysis between energy consumption and communication quality of wireless transceivers.

Individual power models for several transceiver components exist. These include models for analog-to-digital converters (ADCs) and RF power amplifiers. The ADC power model proposed in [11], considers the effect of sampling frequency, signal frequency, and resolution bits but not the signal peak-to-average ratio (PAR). Power amplifier models for Class A, B, AB, and E are proposed in [12] and [13], which show the effect of the power gain, average power, and maximum power consumption. However, the power dissipated in the power amplifier is also related to communication parameters, such as transmission distance, antenna gain, constellation size, channel noise, PAR, and BER; the impact of these parameters have not been considered in the existing models.

Several system level transceiver energy models have also been proposed in recent years. For microsensor systems, the transceiver energy model considers the circuit start-up energy in addition to steady-state dissipated energy in [14]. The energy consumption of every component is assumed to be constant. Another high level model was proposed in [1], which divides the transceiver circuitry power into two parts, one related to the instantaneous symbol rate and the other to the highest symbol rate. However, the dissipated circuit power is not only related to the symbol rate, but also to modulation parameters, such as PAR, required resolution in data converters, signal bandwidth, and sampling frequency. In [15], a more comprehensive model is presented, however, most of the RF front-end components are assumed to have constant power consumption, and the power model for power amplifier is gain dependent, and does not take into account signal characteristics such as PAR.

In this paper, a system level power model for RF front-end components of a wireless transceiver is presented. The components include ADC, DAC, reconstruction and anti-aliasing filters, mixers, frequency synthesizer, power amplifier, low noise amplifier (LNA), and baseband amplifier. The proposed

Manuscript received June 15, 2005; revised May 17, 2006 and September 6, 2006. This work was supported in part by the National Science Foundation/I/UCRC Center for Low Power Electronics under EEC9523338 and by the National Science Foundation-ITR under 0325761.

The authors are with the Department of Electrical Engineering, Arizona State University, Tempe, AZ 85287 USA (e-mail: ye.li@asu.edu; bertan@asu.edu; chaitali@asu.edu).

Digital Object Identifier 10.1109/TVLSI.2007.891095

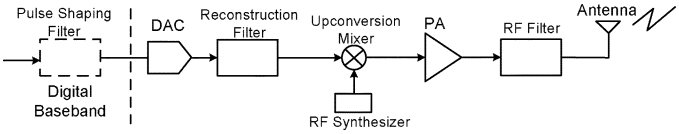

Fig. 1. Block diagram of the transmitter analog signal chain.

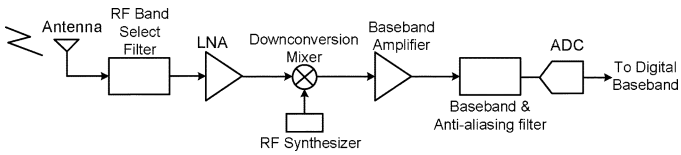

Fig. 2. Block diagram of the receiver analog signal chain.

model is scalable with respect to effects of signal bandwidth, PAR, symbol rate, and data converter sampling frequency. Next, the energy consumption and communication quality of three representative communication systems are evaluated with respect to the effect of these parameters along with constellation size, pulse-shaping filter roll-off factor, multiple access interference (MAI), and IF frequency. The three systems are 1) single user point-to-point communication system such as IS-136 TDMA and GSM; 2) code division multiple access (CDMA)-based multi-user system such as IS-95 and CDMA2000; and 3) receive-only mobile system such as digital video broadcast for handhelds (DVB-H). For single user point-to-point communication systems, the effect of occupied signal bandwidth, PAR, symbol rate, constellation size, and pulse-shaping filter roll-off factor is studied. For CDMA-based multi-user systems, the effect of the number of users in the cell and MAI along with the PAR and filter roll-off factor are analyzed. For receive-only systems, the effect of $1/f$ noise for direct-conversion receiver (DCR) and the effect of IF frequency for low-IF architectures is presented. For a given communication quality specification, a methodology to reduce the energy consumption of the wireless system is presented.

The remainder of this paper is organized as follows. Section II describes the transceiver system model and defines the terminology used in this paper. Section III describes general power models for fundamental components in a wireless transceiver front-end. Section IV analyzes the effect of design parameters on both energy consumption and communication quality of a single user point-to-point wireless data communication system. Section V analyzes energy consumption of a multi-user CDMA system. Section VI describes the energy consumption and communication quality of receive-only communication systems such as DVB-H. Section VII summarizes this paper.

II. System Model for Transceiver

A. Transceiver Building Blocks

In order to minimize the total energy consumption of a transceiver, it is essential to develop accurate energy models for all the key signal processing blocks. The wireless transmitter and receiver model that is used in this model is based on [16] and described in Figs. 1 and 2. The main components of the analog signal chain of the transmitter are DAC, reconstruction filters, upconversion mixers, power amplifiers (PA), and RF filters. Similarly, the main components of the receiver signal chain are the RF band select filter, LNA, downconversion mixers, the baseband amplifier, the baseband and anti-aliasing filters, ADC, and the RF synthesizer. The energy models for each of these components have been described in Section III.

Fig. 1 also shows the placement of the filter for pulse shaping of the baseband signal. The roll-off factor of this filter changes the PAR of the signal and affects both the energy consumption of the RF front-end and the communication quality. In this paper, the energy consumption of the digital pulse-shaping filter is ignored (since it is relatively small) but the effect of the roll-off factor α on the communication quality is considered.

TABLE I
RF Front-End Power Consumption

Component	Active mode	Idle mode	Sleep mode
PA	*126.5 mW*	*0 mW*	*0 mW*
Mixer	*21 mW x2*	*21 mW*	*0 mW*
Freq. Syn.	*67.5 mW x2*	*67.5 mW*	*0 mW*
DAC	*15.4 mW*	*0 mW*	*0 mW*
ADC	*5.85 mW*	*5.85 mW*	*0 mW*
Filters	*5 mW*	*2.5 mW*	*0 mW*
Ref. System	*0.5 mW*	*0.5 mW*	*0.5 mW*
LNA	*20 mW*	*20 mW*	*0 mW*
BA	*5 mW*	*5 mW*	*0 mW*
Total	*355.25 mW*	*122.35 mW*	*0.5 mW*

The power values are under the condition that PAR= 5 dB, $d = 10$ m.

B. Operation Modes for RF Transceivers

In a full-duplex communication system, the transceiver works in the four following modes: active, idle, sleep, and transient mode.

1) *Active:* Both the transmitter and the receiver are fully on. The transmitter modulates the data and sends it through the antenna; the receiver detects, demodulates, and passes packets to the base-band processor.
2) *Idle:* The receiver listens and just passes channel information to the base-band processor.
3) *Sleep:* Most of the circuitry is turned off, except low power consumption blocks, such as the voltage and frequency reference system.
4) *Transient mode:* This occurs when the transceiver switches from sleep mode to active mode, and *vice versa*.

The total energy consumption is the sum of the energy in the four modes and given by

$$E_{\text{total}} = P_{\text{active}}T_{\text{active}} + P_{\text{idle}}T_{\text{idle}} + P_{\text{sleep}}T_{\text{sleep}} + P_{\text{transient}}T_{\text{transient}}.$$

In this paper, only the active energy is considered. Idle mode energy is ignored for the following reasons. Although during the idle mode, all the RF components in the receiving chain are active (see Table I), the duty cycle is assumed to be quite low (see Fig. 3). Furthermore, compared to the power consumed in the active mode, the receive-only idle power consumption is less than one-third. Again, due to the low duty cycle operation, the transient mode energy consumption is also ignored. In many state-of-the-art analog and RF circuits, digital calibration, and

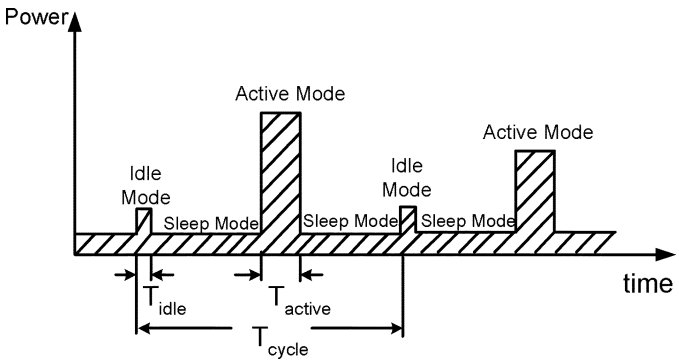

Fig. 3. Power consumption in different modes.

speed-up modes are used to bring the front-end to a fully operational mode quickly, minimizing start-up power consumption. The sleep mode energy consumption which is due to the leakage currents in the RF circuit is also ignored.

The active mode energy consumption can be further divided into two parts: signal transmission energy or radiated energy, which is delivered to the antenna, and dissipated energy which is the energy consumed by the electronic circuits. Since transmission energy is delivered by PA, $P_{\rm PA}$ includes both radiated energy and dissipated energy [15], [16]

$$E_{\rm active} = (P_{\rm PA} + 2P_{\rm mix} + 2P_{\rm FS} + P_{\rm LNA} + P_{\rm filter} + P_{\rm BA} + P_{\rm DAC} + P_{\rm ADC})T_{\rm on} \quad (1)$$

where $P_{\rm PA}$, $P_{\rm mix}$, $P_{\rm FS}$, $P_{\rm LNA}$, $P_{\rm filter}$, and $P_{\rm BA}$ are the power consumption of the PA, mixer, frequency synthesizer, LNA, filters, and baseband amplifier (BA), respectively. The factor 2 before $P_{\rm mix}$ and $P_{\rm FS}$ comes from the assumption that the mixers and the frequency synthesizers have the same power consumption in both the transmitter and the receiver circuitry in a full-duplex system. Note the signal transmitting and receiving chains share a single frequency synthesizer in the half-duplex system.

C. Performance Metrics

In this paper, the performance of the wireless communication node with respect to energy consumption and communication quality is evaluated. The effect of several parameters, including signal bandwidth (BW), signal-to-noise ratio (SNR), PAR, and $1/f$ noise are considered. The communication quality is evaluated in terms of symbol error rate (SER). Several parameters that impact the power consumption are described as follows.

Signal bandwidth is defined as the occupied RF signal spectrum in frequency domain. For m-ary quadrature amplitude modulation (MQAM), both in-phase and quadrature components have the same bandwidth and they are equal to the occupied RF bandwidth.

Noise figure (NF) is a measure of SNR degradation as the signal passes through a signal chain [16]. It is represented by $NF({\rm dB}) = 10{\rm log}({\rm SNR}_{\rm in}/{\rm SNR}_{\rm out})$, where ${\rm SNR}_{\rm in}$ and ${\rm SNR}_{\rm out}$ are the SNRs measured at the input and output points, respectively.

PAR is the ratio of the signal peak power to its ${\rm rms}$ value and is defined as ${\rm PAR(dB)} = 10{\rm log}(P_{\rm Peak}/P_{\rm rms})$. PAR gives information on how the signal is distributed over the amplitude range. A low PAR indicates a more uniform distribution, which is energy efficient. Moreover, as discussed in Sections IV and V, PAR degrades the communication quality of single user point-to-point wireless systems and CDMA-based multi-user systems. Therefore, PAR is an important parameter that affects both energy consumption and communication quality.

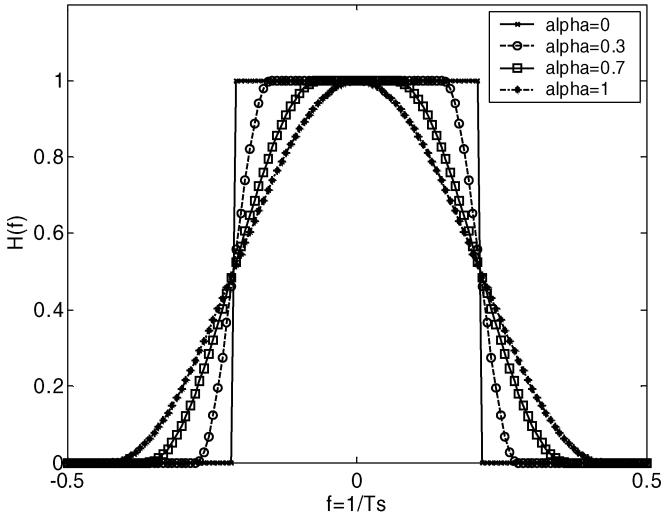

Fig. 4. Frequency response of the pulse-shaping filter for different roll-off factors (α).

There are several existing techniques to reduce the PAR, including clipping [17], block coding [18], and the use of companding transform [19]. However, if raised the cosine pulse-shaping filter is utilized, the values of PAR can also be changed by the roll-off factor of the pulse-shaping filter. Since the pulse-shaping filter can suppress intersymbol interference (ISI) and is one of the basic base-band blocks in most communication systems (dash box in Fig. 1), this technique can be used in addition to the existing techniques.

The raised cosine filter in time-domain can be described by [20]

$$h(t) = \left(\frac{\sin(\pi t/T_s)}{\pi t}\right) \cdot \left(\frac{\cos(\pi\alpha t/T_s)}{1-(4\alpha t/(2T_s))^2}\right)$$

where T_s is the symbol rate and α is the roll-off factor. As described in [20], lower α results in higher amplitude of the side-lobe, and after the signal passes through the pulse-shaping filter, the signal peak value increases due to the convolution process.

Fig. 4 depicts the frequency response of the pulse-shaping filter. Since the signal average power is affected by the effective area of the frequency response of the pulse-shaping filter, from Fig. 4, we can expect that with the variation of α, the signal average power $P_{\rm ave}$ will not change dramatically. Thus, we can conclude that with the increase of roll-off factor α, the PAR will reduce.

Fig. 4 also shows that higher roll-off factor α value results in larger signal bandwidth. When $\alpha = 0$, the frequency response is rectangular, the regrowth bandwidth is zero, and the PAR is the highest. As α increases, the bandwidth increases and the PAR reduces. Therefore, the roll-off factor can be used to control the occupied signal bandwidth and PAR.

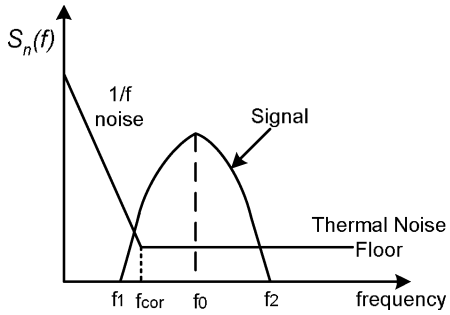

Fig. 5. Power spectral density of $1/f$ noise and thermal noise with respect to occupied signal bandwidth.

PAR is also affected by the modulation level b. The relation between PAR and modulation level b can be expressed as [21]

$$\mathrm{PAR}_{\mathrm{modulation}}(\mathrm{dB}) = 10 \cdot \log\left(\sqrt{\frac{3\cdot\left(2^{b/2}-1\right)}{\left(2^{b/2}+1\right)}}\cdot \mathrm{PAR}_C\right)$$

where PAR_C is the PAR of the carrier. If the carrier is a sine wave, $\mathrm{PAR}_C = 1.4$. This equation also shows that PAR increases with modulation level b.

Thus, PAR is a function of both modulation level b and roll-off factor α, and the two parameters are independent

$$\begin{aligned}\mathrm{PAR}(\mathrm{dB}) &= \mathrm{PAR}_{\mathrm{modulation}}(\mathrm{dB}) + \mathrm{PAR}_{\mathrm{roll-off}}(\mathrm{dB})\\ &= 10\cdot\log\left(\sqrt{\frac{3\cdot\left(2^{b/2}-1\right)}{\left(2^{b/2}+1\right)}}\cdot \mathrm{PAR}_C\right)\\ &\quad + \mathrm{PAR}_{\mathrm{roll-off}}(\mathrm{dB}).\end{aligned}$$

$1/f$ noise is an intrinsic noise phenomenon found in semiconductor devices with a -10 dB/dec frequency dependency in power. We define the power spectral density $V_n^2(f)$ of $1/f$ noise as

$$V_n^2(f) = \frac{K_v}{f}$$

where K_v is a device dependent constant. From the previous equation, we can see that $1/f$ noise can dominate the base-band noise budget in direct conversion receivers. The intersection of the $1/f$ and thermal noise curves is often referred to as the *corner frequency* f_{cor}.

Fig. 5 shows the power spectral density of $1/f$ noise and thermal noise. The signal bandwidth is $BW = f_2 - f_1$, f_0 is the signal center frequency, and N_0 is the thermal noise floor. At the corner frequency f_{cor}, we have

$$N_0 = \frac{K_v}{f_{\mathrm{cor}}}.$$

The integrated noise power, including the effect of both $1/f$ noise and thermal noise can be estimated as

$$\begin{aligned}N_{\mathrm{integ}} &= N_0\cdot(f_2-f_1) + \int_{f_1}^{f_2}\frac{K_v}{f}df\\ &= N_0\cdot\left[BW + f_{\mathrm{cor}}\cdot\ln\left|\frac{f_0+BW/2}{f_0-BW/2}\right|\right]. \qquad (2)\end{aligned}$$

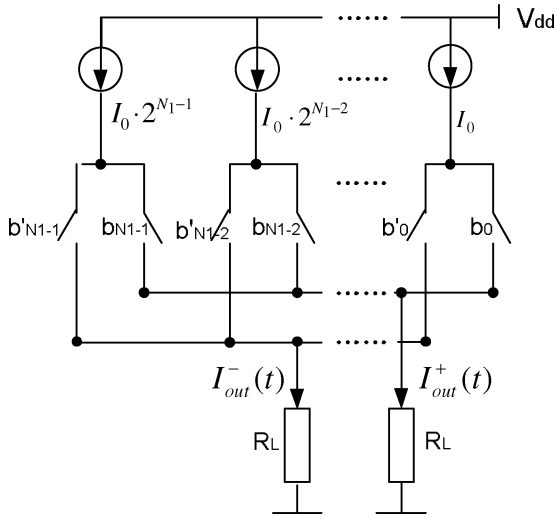

Fig. 6. Binary-weighted current steering DAC with differential switches.

Thus, integrated noise is affected by both the signal bandwidth and center frequency. As the modulated signal is moved to low IF bands, the impact of $1/f$ noise on SNR can be reduced. In this paper, we assume that the integrated noise has a Gaussian distribution. For a superheterodyne receiver, $1/f$ noise is negligible because the signal is substantially amplified by IF gain and filtering stages. When the amplified signal is downconverted to baseband, $1/f$ noise becomes insignificant relative to the signal power. However, for a direct-conversion system which has useful signal around dc with minimum filtering, $1/f$ noise degrades the communication quality.

III. Power Model

In this section, the power models for each of the components in the analog signal chain of a transceiver are presented. The existing power models for ADC [11], DAC [21], and class A PA [12] have been enhanced and new models have been developed for the phase-locked loop (PLL) and voltage-controlled oscillator (VCO).

A. DAC Power Model

The DAC converts the digital signal obtained at the output of the digital modulation block to analog signal. It is the first block in the analog signal chain of the transmitter.

In this model, a current-steering DAC architecture with differential switches is used, in which the binary scaled current is always on and routed to the output load or to the ground (Fig. 6). The DAC power consumption is related to PAR, SQNR, signal bandwidth, and resolution. It can be divided into two parts: the static power consumption P_s and the dynamic power consumption P_d. According to Fig. 6, the power of the current sources can be calculated as

$$P_s = V_{\mathrm{dd}}\cdot I_0\cdot E\left[\sum_{i=0}^{N_1-1}2^i\right] = V_{\mathrm{dd}}\cdot I_0\cdot\left(2^{N_1}-1\right)$$

where V_{dd} is the power supply and N_1 is the resolution bits. I_0 is the unit current source per LSB, which is a constant value for a given DAC. In this paper, we assume $I_0 = 5$ uA.

The dynamic power model is similar to [24], with the signal centered around dc. For the N_1 switches in Fig. 6, P_d can be calculated as

$$P_d = 0.5 \cdot N_1 \cdot C_p \cdot \text{OSR} \cdot B \cdot V_{\text{dd}}^2$$

where C_p is the parasitic capacitance of each switch, the factor 0.5 is the value of switching probability during a symbol transition. B is the signal bandwidth and OSR is the oversampling rate representing the ratio between signal bandwidth and sampling rate. Higher OSR reduces the reconstruction filter requirements, moving the Nyquist images further out. For the proposed model, OSR$= 4$.

In data converters, the resolution N_1 can be expressed in terms of SQNR and signal PAR as shown in [21]

$$N_1 = \frac{\text{SQNR(dB)} + \text{PAR(dB)} - 4.77\ \text{dB}}{6.02}. \tag{3}$$

Thus, the total power consumption of DAC, P_{DAC}, can be expressed as a function of PAR, SQNR, signal bandwidth B, and resolution N_1 as follows:

$$\begin{aligned} P_{\text{DAC}} = {} & V_{\text{dd}} \cdot I_0 \cdot \left(2^{\text{SQNR(dB)}+\text{PAR(dB)}-4.77\text{dB}/6.02} - 1\right) \\ & + 0.5 \cdot \frac{\text{SQNR(dB)} + \text{PAR(dB)} - 4.77\ \text{dB}}{6.02} \\ & \cdot C_p \cdot \text{OSR} \cdot B \cdot V_{\text{dd}}^2. \end{aligned} \tag{4}$$

B. Analog Filter Power Model

There are several analog filters in a transceiver front-end. These include the reconstruction filter of the DAC, RF filter in the transmitter, RF band select filter, and the base-band and anti-aliasing filter in the receiver. The reconstruction filter in the transmitter suppresses the Nyquist images due to zero order hold (ZOH) operation of the DAC. The RF filter at the output of the PA helps with suppression of spurious emissions and thermal noise floor from transmitter circuitry. At the receiver, the RF band select filter suppresses wideband interference signals and helps with the linearity of the receiver. Base-band filters suppress in-band interference and help with anti-aliasing filtering for the ADC.

We can estimate the baseband active analog filter power consumption as follows [22]:

$$P_{\text{filter}} = n \cdot kT \cdot Q \cdot f_0 \cdot \text{SNR}^2 \tag{5}$$

where n is a proportionality constant depending on the filter topology and the active elements used (op-amp RC, transconductance-C, etc.), Q is the quality factor, f_0 is the center frequency (band-pass filter) or corner frequency (low-pass filter), and SNR is the signal-to-noise ratio of the filter.

Similar filter types have been used for both the transmit and receive base-band chains. If a direct downconversion receiver and direct upconversion transmitter is utilized, the power model for the analog filter can be used to calculate the majority of active filters used in transmit and receive chain of an RF transceiver. The power consumption of the analog filter is related to the in-band SNR, linearity, roll-off characteristics (quality factor), and signal center frequency. Passive RF filters such as ceramic and surface acoustic wave (SAW) filters have not been included in the transceiver power model, since they do not consume quiescent power and their specifications are not directly related to base-band modulation requirements.

C. Frequency Translation Circuits

Frequency translation (upconversion and downconversion) in RF transceivers are performed with mixers. This frequency translation is a result of time-domain multiplication of high frequency input signal (RF input) with a spectrally clean local oscillator (LO) signal. The LO signal is generated by a PLL synthesizer coupled with a VCO. In the following sections, RF PLL building blocks as well as mixer power consumption is modeled with respect to frequency of LO (F_{LO}), reference frequency (F_{ref}) and LO signal swing.

1) PLL Power Consumption: The most critical building blocks that consume quiescent current for a PLL frequency synthesizer are the multi-modulus feedback divider (MMD), charge-pump phase-frequency detector (PFD), and in the case of fractional-N PLLs, the fractional controller. For narrowband communication systems, where RF center frequency F_{LO} is much higher than the occupied bandwidth of the modulated signal BW, the power consumption of a PLL with frequency multiplication ratio of N can be estimated as follows:

$$P_{\text{pll}} = b_1 \cdot C_1 \cdot V_{\text{dd}}^2 \cdot F_{\text{LO}} + b_2 \cdot C_2 \cdot V_{\text{dd}}^2 \cdot F_{\text{ref}} \tag{6}$$

where C_1 and C_2 represent the total parasitic capacitance loading of the RF circuits, F_{ref} is the reference frequency and V_{dd} is the supply voltage, which is also assumed to be equivalent to the LO voltage swing. The first term in (6) predicts power associated with frequency dividers as well as buffers working at F_{LO} frequency. b_2 is the proportionality constant that is a function of the process, and includes impact of phase detector, as well as clock reference buffers, charge pump PFD. In the case of fractional-N PLLs, the $\Sigma\Delta$ modulator controller for the divider also adds to this power consumption number. The b_2 term is, therefore, bigger in fractional-N PLLs compared to integer PLLs.

A detailed PLL power model has also been proposed in [25]. In comparison, the PLL power presented represented by (6) does not include the power consumption of the PLL start-up separately. The proposed model assumes that there is a start-up calibration cycle that enables a fast locking behavior.

2) VCO Power Consumption: VCO phase noise determines the far-out phase noise of the LO signal and has direct impact on the receiver noise figure (NF) and transmit signal quality (EVM and transmit signal mask requirements). Low phase noise is a critical requirement for RF VCOs since power consumption is usually inversely proportional to phase noise in these VCOs. In this paper, LC-tank-based VCOs are considered, since they provide lower phase noise at lower signal swings.

A general LC-tank-based VCO is symbolized in Fig. 7. The oscillator consists of a parallel resonant tank built by an inductor

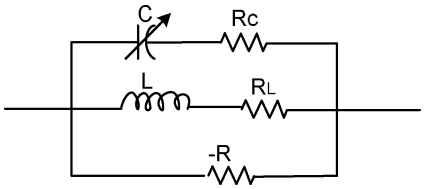

Fig. 7. LC tank-based VCO model.

L, capacitor C, with an active element denoted by negative resistance $-R$ compensating for tank losses. The voltage dependent capacitor C (varactor) tunes the center frequency ω_c of the VCO yielding $\omega_c = (1/\sqrt{LC})$.

Using energy conservation, the peak energy stored in the inductor and the capacitor should be equal $(C \cdot V_{\rm pk}^2)/2 = (L \cdot I_{\rm pk}^2)/2$, where $V_{\rm pk}$ and $I_{\rm pk}$ is the peak voltage and current amplitude inside the tank circuit. The power loss in the tank resistor can be calculated as

$$\text{Pvco} = R \cdot I_{\rm pk}^2 = C\frac{R}{L}V_{\rm pk}^2 = RC^2\omega_c^2 V_{\rm pk}^2 = \frac{R}{L^2\omega_c^2}V_{\rm pk}^2. \quad (7)$$

As shown in (7), the power consumption of a VCO increases with peak signal swing. For a given series resistance, the efficiency can be increased by increasing the inductance. For an MQAM communication system, the LO phase noise plays an important role in received signal quality (EVM). Utilizing Leeson's model, the phase noise power spectral density S_Φ for an LC-tank-based VCO follows:

$$S_\phi = \text{NEF} \cdot \frac{k \cdot T}{2 \cdot P_{\rm sig}} \cdot \frac{\omega_c^2}{Q^2 \Delta\omega^2} \quad (8)$$

where NEF is the noise excess factor of the active device used in the oscillator, Q is the quality factor of the LC tank, $P_{\rm sig}$ is the ac signal power of the oscillation waveform, and $\Delta\omega$ is the offset frequency from the carrier. An obvious method to reduce phase noise is to increase signal swing. However, this will increase oscillator power consumption quadratically, as shown in (7). Another critical parameter to reduce the phase noise of the oscillator is the tank quality factor Q

$$Q = \frac{1}{R}\sqrt{\frac{L}{C}} = \frac{L}{R}\omega_c. \quad (9)$$

Utilizing (7), we can get a relationship between the power consumption and single-side-band phase noise of an electrical oscillator. Solving for $P_{\rm sig}$ in (8), we have

$$P_{\rm sig} = \text{NEF} \cdot \frac{k \cdot T}{2 \cdot S_\phi} \cdot \frac{\omega_c^2}{Q^2 \cdot (\Delta\omega)^2}.$$

Solving for $P_{\rm vco}$ in (7) for $P_{\rm sig} = V_{\rm pk}^2/2$

$$P_{\rm VCO} = C \cdot \left(\frac{R}{L}\right)^3 \cdot \text{NEF} \cdot \frac{k \cdot T}{S_\phi} \cdot \frac{1}{(\Delta\omega)^2}. \quad (10)$$

For a given MQAM system, SNR and EVM, phase noise requirements (S_Φ, as well as oscillation frequency for the LO are fixed. In the proposed power model, EVM specifications and constellation size have been used to derive VCO phase noise requirements [39]. Phase noise is then used to estimate VCO power consumption for a state-of-the-art LC-tank oscillator quality factor.

D. LNA and Mixer Power Model

There are two mixers in the transceiver. The upconversion mixer in the transmitter moves the base-band signal to a higher frequency. The downconversion mixer in the receiver demodulates the RF signal from RF to baseband.

The power model of the mixer is a function of the noise figure NF and the gain K [23]

$$P_{\rm mixer} = k_{\rm mixer} \cdot K/NF. \quad (11)$$

LNA amplifies the received signals with low input referred noise. LNA determines the overall noise figure of the receiver. The power model of an LNA is similar to that of the mixer. It is also a function of the noise figure NF and the gain A [23]

$$P_{\rm LNA} = k_{\rm LNA} \cdot A/NF. \quad (12)$$

Note that the NF and gain of an LNA is optimized for the full receiver bandwidth. Therefore, the power consumption of the LNA and mixer is not a function of the occupied RF bandwidth, but the overall receive channel bandwidth.

E. PA Model

The PA increases the signal power so that the antenna can radiate sufficient power for a reliable communication. The proposed model utilizes Class A linear PAs, since they are commonly used in QAM-based single user point-to-point systems. The high linearity of this amplifier preserves communication accuracy and limits spectral regrowth.

The efficiency η of Class A PA is proportional to the rms value of the output power [12]

$$\eta = \frac{P_{\rm rms}}{P_{\rm PA}} = \frac{K}{\text{PAR}} \quad (13)$$

where $P_{\rm rms}$ is the output power and K is a proportionality constant. We choose $K = 0.5$ in our simulation.

Therefore

$$P_{\rm PA} = \frac{P_{\rm rms}}{K} \cdot \text{PAR}. \quad (14)$$

where $P_{\rm rms}$ is proportional to the detected signal power $P_{\rm detected}$ at the receiver, the antenna gain, and the propagation distance. According to [20], the symbol error rate at the receiver can be expressed as

$$\text{SER} = 4\left(1 - \frac{1}{\sqrt{M}}\right) \cdot Q\left(\sqrt{\frac{3 \cdot P_{\rm detected}}{(M-1) \cdot N}}\right) \quad (15)$$

TABLE II
RF POWER CONSUMPTION FOR DIFFERENT BLOCKS IN THE RF FRONT-END OF A TRANSCEIVER

Components	Power Model Parameters	Exemplary power	*PAR=10dB*	*PAR=3dB*
PA	*PAR, d, b, SER*	5270mW[27[1]]	*400 mW*	*79.8 mW*
Mixer	*K,NF*	21mW[28]	*21mW*	*21mW*
Freq. Syn.	$\omega_c, F_{LO}, F_{ref}$	52mW[29]+ 15.18mW[30]	*67.5mW*	*67.5mW*
LNA	*A, NF*	*21mW[31]*	*20mW*	*20mW*
ADC	*PAR, SNR, f*	*4.5mW[32]*	*7.8mW*	*5.2mW*
DAC	*PAR,SNR*	*24 mW[33]*	*27.4mW*	*12.2mW*
Filter	*f, SNR*	*3.9mW[34]*	*5mW*	*5mW*
BA	*B,* α_{BA}	*7.2mW[35]*	*5mW*	*5mW*

$P_{\rm rms} = 13$ dBm; PAR is the peak-to-average ratio; SNR is the signal-to-noise ratio; SER is the symbol error rate; d is the transmission distance; b is the number of bits per symbol; K is the gain of the mixer; NF is the noise figure; ω_c is the center frequency of VCO; $F_{\rm LO}$ is the frequency of the local oscillator; $F_{\rm ref}$ is the reference frequency; A is the gain of LNA; f is the signal frequency of ADC; B is the bandwidth of the base-band amplifier; $\alpha_{\rm BA}$ is the gain of the base-band amplifier.

[1]The PA power consumption in the reference is the maximum value. However, most of the time PA output power is much lower than the maximum value. For example, the output power of a linear PA for IS-95 CDMA system varies between -5 and 15 dBm [40]. In our proposed model, the PA power consumption is 138.13 mW with a 13-dBm output power.

where N is the noise power and M is the constellation size. Therefore

$$P_{\rm detected} = \frac{1}{3}(2^b - 1) \cdot N \cdot \left(Q^{-1} \left(\frac{1}{4} \left(1 - \frac{1}{2^{b/2}} \right)^{-1} {\rm SER} \right) \right)^2 .$$

Assuming free space propagation at distance d (meter), the average transmission power $P_{\rm rms}$ is given by [20]

$$P_{\rm detected} = \frac{P_{\rm rms} G_t G_r \lambda^2}{(4\pi)^2 \cdot d^2 \cdot L} \tag{16}$$

where G_t and G_r are the transmitter and receiver antenna gain, L is the system loss factor not related to propagation, and λ is the carrier wavelength. The power consumption of the PA is thus given by

$$P_{\rm PA} = \frac{16 \cdot \pi^2 \cdot d^2 \cdot L}{3 G_r G_t \lambda^2 \cdot K} (2^b - 1) \cdot N \cdot \left(Q^{-1} \left(\frac{1}{4} \left(1 - \frac{1}{2^{b/2}} \right)^{-1} {\rm SER} \right) \right)^2 {\rm PAR}. \tag{17}$$

F. Base-Band Amplifier (BA) Power Model

After downconversion, an IF (or baseband) low-noise amplifier is used to provide gain for signal before A/D conversion. Larger signal amplitudes give a higher SNR in the ADC and improve the receiver BER. Depending on the receiver linearity requirements, multiple filter and gain stages may be necessary to suppress in-band interferers. As shown in [15], the power consumption of the base-band amplifier is proportional to the gain and its bandwidth

$$P_{\rm BA} = k \cdot (B + f_o) \cdot \sqrt{a_{\rm BA}} \tag{18}$$

where the coefficient k is decided by device dimensions and other process parameters, and f_0 is the center frequency (see Section II-C). $a_{\rm BA}$ is the baseband amplifier gain and is assumed to be $a_{\rm BA} = 5$.

G. ADC Power Model

The ADC converts the base-band analog signal to the base-band digital signal in the receiver. If Nyquist-rate ADC is used in the transceiver, we can use an accurate power estimation model based on [11]. The power consumption of ADC can be calculated as follows:

$$P_{\rm ADC} = \frac{V_{\rm dd}^2 \cdot L_{\rm min} \cdot (f_{\rm sample} + f_{\rm signal})}{10^{(-0.1525 \cdot N_1 + 4.838)}}$$

where N_1 is the resolution of the A/D converter, $L_{\rm min}$ is the minimum channel length for the given CMOS technology. For our analysis, we assume $L_{\rm min} = 0.4$ μm and $V_{\rm dd} = 3$ V, and N_1 is a function of PAR shown in (3)

$$P_{\rm ADC} = \frac{V_{\rm dd}^2 \cdot L_{\rm min} \cdot (f_{\rm sample} + f_{\rm signal})}{10^{-0.0253 \cdot ({\rm SQNR} + {\rm PAR}) + 4.959}}. \tag{19}$$

H. Power Model Summary

Table II summarizes the effect of different parameters that contribute to power consumption of different front-end components. For instance, Class A power amplifier is a function of PAR, distance d, number of bits per symbol b, and symbol error rate SER. Table II also lists the power consumption of the different components in an RF front-end for two values of PAR: 3 and 10 dB. We see that while the PA power is less dominant at lower PAR values, it is by far the largest component for high PAR. As a comparison, exemplary power values from most commonly referred publications are listed in Table II.

TABLE III
SIMULATION ENVIRONMENT

$B=1MHz$	$Gr=1$
$Gt=1$	$L=0.8$
$f_c=2.5GHz$	$\lambda=0.12m$
$\alpha=0.5$	$K=0.5$
$N_0/2=10^{-16}W/Hz$	$BER=10^{-4}$
$d=10m$	$b_{default}=4$
$SQNR_{ADC}=50dB$	$SQNR_{DAC}=60dB$
$OSR_{DAC}=4$	$I_{0\_DAC}=10uA$

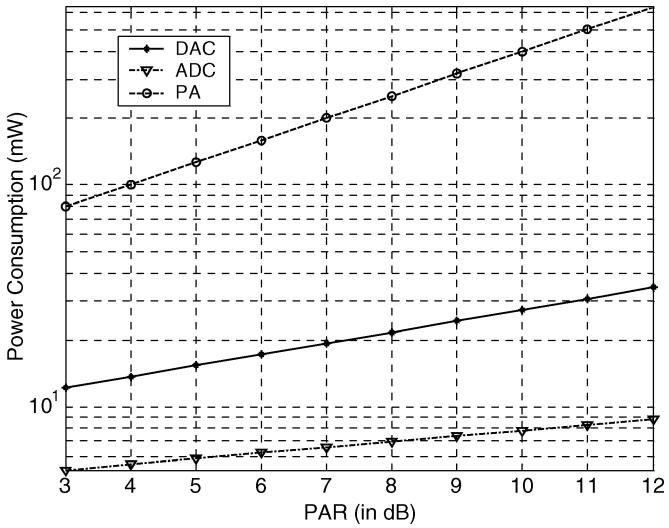

Fig. 8. Power consumption of PA, ADC, and DAC for different PAR; transmission power $P_{\rm rms} = 13$ dBm, 16 QAM modulation, $d = 10$ m.

In Table II, power consumption of PAR sensitive components are simulated according to the parameters shown in Table III, while the other assumed power values are in a reasonable range compared with the published power values.

IV. SINGLE USER WIRELESS DATA COMMUNICATION SYSTEM

In this section, a single user wireless communication system, similar to IS-136 time division multiple access (TDMA) and global system for mobile communication (GSM), is studied. We assume that MQAM is used as the modulation scheme, and because of the linearly requirement of MQAM, the Class A PA is adopted. Since PA is the dominant power source and is PAR sensitive, the effect of PAR on the communication quality and the energy consumption of such a system are evaluated.

A. Energy Consumption

From the power models described in Section III, we see that PAR directly affects the power consumption of PA, ADC, and DAC. The power consumption of filters, mixer, frequency synthesizer, and LNA is not directly affected by PAR. Fig. 8 illustrates the effect of PAR on the power consumption of the PA, ADC, and DAC. It is clear that the power consumption increases with PAR, and that the PA power is impacted the most. For example, the PA power increases by more than a factor of 3.16

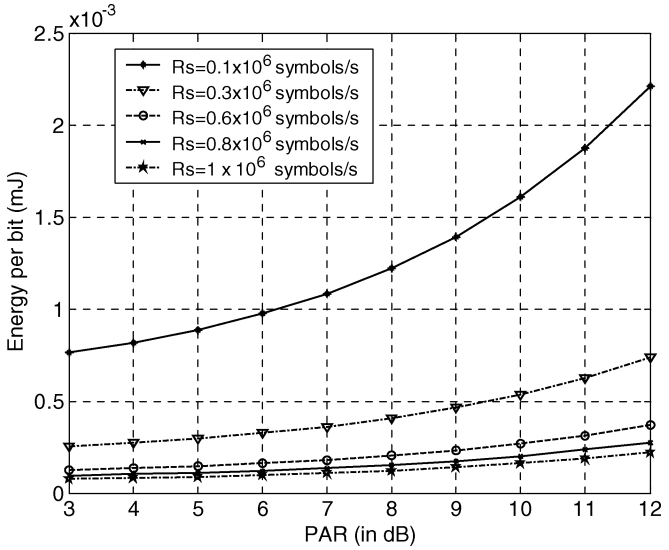

Fig. 9. Active energy consumption per bit for 16 QAM for different values of PAR, transmission power; $P_{\rm rms} = 13$ dBm, $d = 10$ m.

(159.2 to 536 mW) when the PAR increases from 6 to 11 dB. In comparison, the ADC power consumption increases by a factor of 1.34 and the DAC power increases by a factor of 1.78. Fig. 8 also shows that the power consumption of PA is much more than that of ADC and DAC.

The rest of this section presents the evaluation results for the energy performance of the system with respect to the active energy per bit, $E_{\rm bit}$

$$\begin{aligned} E_{\rm bit} &= (P_{\rm non-PAR} + P_{\rm PAR})T_{\rm bit} \\ &= (2P_{\rm mixer} + 2P_{\rm FS} + P_{\rm LNA} + P_{\rm filter} + P_{\rm BA})/(R_s b) \\ &\quad + (P_{\rm PA} + P_{\rm ADC} + P_{\rm DAC})/(R_s b). \end{aligned} \tag{20}$$

Here $P_{\rm PAR}$ represents the sum of the power of the components related to PAR and $P_{\rm non-PAR}$ represents the sum of the power of the components not related to PAR. R_s is the symbol rate and b is the number of bits in one symbol ($b = \log_2 M$).

Fig. 9 shows the effect of PAR and the symbol rate R_s on the active energy per bit, $E_{\rm bit}$, for $b = 4$. For fixed R_s and fixed b (*bits/symbol*), $E_{\rm bit}$ increases with PAR. This is because the power consumption of PA, ADC, and DAC increases with increased PAR (Table II). If we further fix PAR and compare $E_{\rm bit}$ for different symbol rates, we can see that as the symbol rate increases, the energy consumption reduces. The trend is similar to that in [1].

Fig. 9 also shows that $E_{\rm bit}$ can be reduced by operating the system at high symbol rates. Higher symbol rate results in shorter bit duration ($T_{\rm bit} \propto 1/R_s$), which results in reduced analog circuitry energy. If the symbol rate is low, it is even more important that the PAR be kept as low as possible.

Next, the effect of b, the number of bits per symbol (for a fixed symbol rate R_s), on $E_{\rm bit}$ is compared. While the PA energy consumption increases with transmission distance d and b (*bits/symbol*) [see (17)], the active energy of other components is inversely proportional to b [see (20)]. For small values of b, PA energy consumption is low and $E_{\rm bit}$ reduces with increase in b (*bits/symbol*). For higher b (*bits/symbol*), PA energy consumption becomes dominant and $E_{\rm bit}$ increases. For a specific value

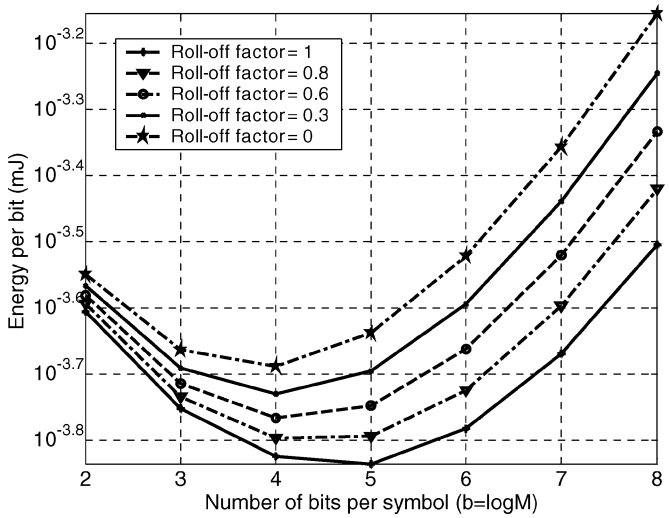

Fig. 10. Energy consumption for different b (*bits/symbol*), $d = 10$ m, $R_s = 0.5$ MHz.

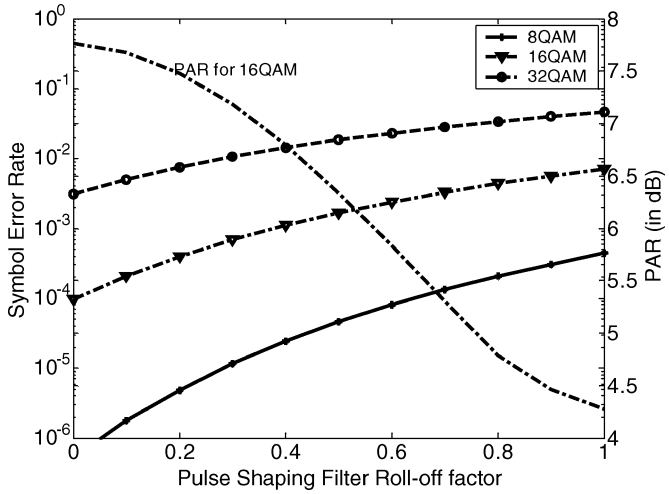

Fig. 11. Single user MQAM system: SER and PAR versus α, $d = 10$ m; PAR curve is plotted by randomly generated 16 QAM signal.

of α, there is an optimal value of b_{opt} (*bits/symbol*) for which E_{bit} is the minimum. This optimum is demonstrated in Fig. 10 for transmission distance $d = 10$ m.

The relation between E_{bit} and b (*bits/symbol*) for different α is also considered. As α decreases, the optimal value of b reduces. This is because as α decreases (PAR increases), the PA power becomes dominant for lower values of b (*bits/symbol*). The effect of PAR on energy consumption and quality has not been considered in [15].

For a fixed α, the E_{bit} trends presented here are similar to [15] and [26]; when the transmission distance is low; E_{bit} reduces as b increases for small b, and then increases for larger b.

As the transmission distance increases, the optimal b (*bits/symbol*) corresponding to minimum E_{bit} also reduces. This is because as the distance increases, the impact of PA energy increases.

B. Communication Quality

Next, the communication quality (SER) of a point-to-point wireless data communication system based on MQAM is presented. As shown in Section II-C, PAR can be adjusted by changing the roll-off factor α of the pulse shaping filter. Note that α changes the signal bandwidth by a factor of $(1 + \alpha)$ [20]. If the bandwidth of the low-pass filter in the receiver is the same as signal bandwidth and the received signal power is kept the same, the noise power equals

$$N = 2B\sigma^2 \cdot NF = 2R_s(1+\alpha) \cdot \sigma^2 \cdot NF \qquad (21)$$

where σ^2 is the single-sided noise power spectral density and NF is the noise figure. Combining (15) and (21), we have

$$\text{SER} = 4\left(1 - \frac{1}{\sqrt{M}}\right) \cdot Q\left(\sqrt{\frac{3 \cdot P_{\text{detected}}}{(M-1) \cdot 2R_s(1+\alpha) \cdot \sigma^2 \cdot NF}}\right)$$

where $Q(x) = 1/\sqrt{2\pi}\int_x^\infty e^{-y^2/2}dy$.

Assuming

$$\text{SNR}_0 = \frac{P_{\text{detected}}}{2R_s\sigma^2 \cdot NF}. \qquad (22)$$

We obtain

$$\text{SER} = 4\left(1 - \frac{1}{\sqrt{M}}\right) \cdot Q\left(\sqrt{\frac{3 \cdot \text{SNR}_0}{(M-1) \cdot (1+\alpha)}}\right). \qquad (23)$$

Equation (23) establishes the relationship between SER and parameters α and M. Fig. 11 shows how SER increases with the increase in roll-off factor α for different constellation sizes, $M = 8$, 16, 32. The increase in SER can be explained as follows: the increase in α expands the signal bandwidth and makes the integrated noise power increase. Fig. 11 also demonstrates the effect of α on the PAR. For a given M, as α increases, PAR reduces causing E_{bit} to reduce as well (see Fig. 10).

C. Low Energy System Design for a Specified SER

The previous analysis can be used to design a low energy system with a given SER specification. From Fig. 11, we can find multiple combinations of roll-off factor α and constellation size M that satisfy the SER requirement. For each candidate combination (α, M), the active energy per bit, E_{bit}, can be compared to Fig. 10 and then the one with minimum E_{bit} can be chosen. Thus, for a given SER, the system roll-off factor α and b (*bits/symbol*) corresponding to the minimum energy configuration can be determined. Note that the minimum energy configuration changes with distance d.

V. Spread Spectrum Multi-User Wireless Communication System

This section presents the performance evaluation of a wireless transceiver in a CDMA-based multi-user wireless communication system, such as IS-95 and CDMA 2000. When the number of users is low, the dominant cause for interference is thermal noise, which is similar to point-to-point single user communication system. However, if the number of users is high, the dominant cause of interference is not thermal noise, but MAI

from other users. This is why thermal noise is typically ignored in high capacity DS-CDMA performance evaluation [35], [36]. But for wireless transceiver design with a variable number of users, it is important to consider the effect of both thermal noise and MAI.

A. Communication Quality

This section demonstrates the effect of thermal noise, MAI, and the number of users in the cell on the communication quality (SER). We assume that BPSK modulation is used. The MAI related component is modeled as a zero-mean Gaussian random variable with a variance of $Var(MAI)$. The thermal noise related component is also modeled as a zero-mean Gaussian random variable with a variance of $Var(N)$. We choose the standard Gaussian approximation (SGA) [35], [36] to evaluate SER. According to SGA, and the probability of bit error rate (for BPSK, BER=SER) of any user can be expressed as [37]

$$\text{SER} = Q\left([Var(N) + Var(MAI)]^{-\frac{1}{2}}\right) \tag{24}$$

where $Q(x) = 1/\sqrt{2\pi}\int_x^\infty e^{-y^2/2}dy$, $Var(N) = (N_0/2E_{\text{bit}})$, and N_0 are the noise power spectral density.

According to (21) and (22), we have

$$Var(N) = \frac{N_0}{2E_{\text{bit}}} = \frac{1+\alpha}{2\cdot \text{SNR}_0}.$$

The variance of MAI is given by [36]

$$Var(MAI) = \frac{S-1}{2\cdot PN}\left(1-\frac{\alpha}{4}\right)$$

where S is the number of users in the system and PN is the length of the spread spectrum sequence. So SER can be expressed as

$$\text{SER} = Q\left(\left[\frac{1+\alpha}{2\cdot \text{SNR}_0} + \frac{S-1}{2\cdot PN}\left(1-\frac{\alpha}{4}\right)\right]^{-\frac{1}{2}}\right). \tag{25}$$

Fig. 12 describes how SER changes with roll-off factor α as the number of users in the system changes. It also shows the effect of MAI and thermal noise on SER for a different number of users. For a CDMA-based multi-user system with fixed roll-off factor α, as the number of users increase, the communication quality due to MAI deteriorates. When the number of users is more than 10,[1] MAI is dominant and SER reduces with the increase in roll-off factor α. For instance, if the number of users is 50, SER reduces from 0.0734 for $\alpha = 0.2$ to 0.0654 for $\alpha = 0.6$ (see Fig. 12). The reduction is because lower PAR (corresponding to greater α) introduces less MAI interference to other users in the same system—a trend that has also been demonstrated in [35] and [36]. However, when the number of users is low (less than 10), MAI is not as important as thermal noise and SER increases with roll-off factor α (dashed line in Fig. 12). For instance, as shown in Fig. 12, when the number of users approaches 10, SER increases from 6.98×10^{-4} for $\alpha = 0.2$ to 8.18×10^{-4} for $\alpha = 0.6$. This trend is similar to that of point-to-point communication (Section IV-B). However, if only MAI is considered for such a system (dashed line in Fig. 12), we may conclude that SER reduces with α which is not correct.

[1]10 is the approximate solution for the differential equation $(\partial \text{SER}/\partial S) = 0$.

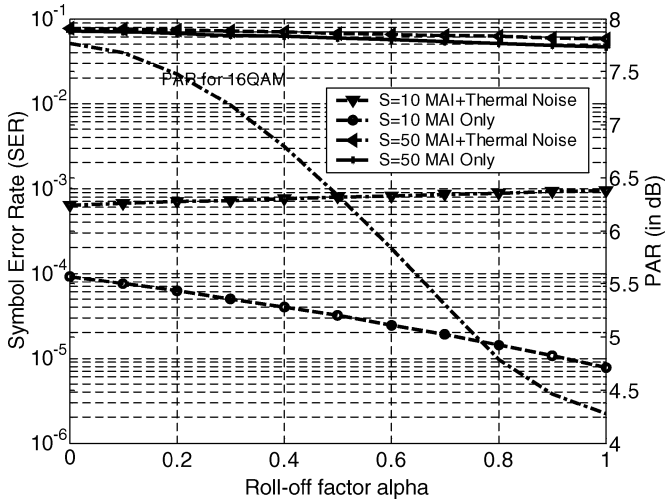

Fig. 12. CDMA-based multi-user system: SER and PAR versus α, $PN = 63$; PAR curve is plotted by randomly generated 16 QAM signal.

B. Energy Consumption

Although a CDMA system works at a higher center frequency and wider modulation bandwidth, its RF front-end is similar to a single user point-to-point communication system. Consequently, the effect of PAR on the front-end energy is similar, and higher PAR introduces higher energy consumption.

C. Low Energy System Design for Specified SER

The previous analysis can also help design a low energy CDMA wireless transceiver for a given SER. The number of users in the system must be considered since it determines whether MAI is the dominant source of SER degradation.

For a multi-user CDMA system with more than ten users, PAR reduction helps in reducing front-end energy consumption and in enhancing communication quality. This comes at the price of increase in occupied signal bandwidth. Therefore, PAR (roll-off factor α) is an important control knob for the tradeoff between energy and occupied signal bandwidth. On the contrary, for a CDMA system with less than ten users, PAR (roll-off factor α) has the inverse effect on front-end energy consumption and communication quality, and PAR is a critical control knob for establishing the tradeoff between them.

VI. Receive-Only Systems

This section studies the energy and communication quality tradeoffs for receive-only systems, such as digital video broadcast for handhelds (DVB-H).

For DVB-H, 16 QAM is assumed for the analysis and because of the power constraints; both direct-conversion receiver (DCR) and low-IF downconversion are considered. While use of DCR allows us to remove IF analog components and thereby lower power, after downconversion from RF to baseband, the signal is subjected to $1/f$ noise in base-band amplifier, base-band analog filter, and ADC. As an alternative, to avoid $1/f$ noise, the signal

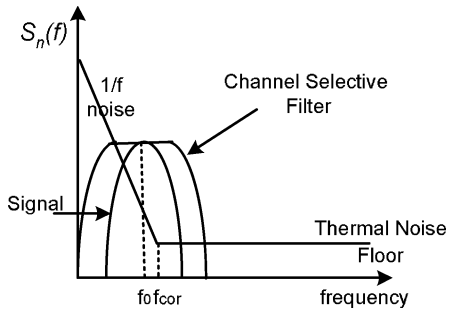

Fig. 13. Low IF downconversion to reduce the impact of $1/f$ noise.

TABLE IV
SIMULATION ENVIRONMENT FOR RECEIVE-ONLY SYSTEM

BW=1MHz	*Center Frequency f_0=3~10MHz*
SNR=12dB	*Default modulation level b=4*
f_{cor}=0.2BW	*NF=10dB*
α=0.5	*Sensitivity = -103dBm*

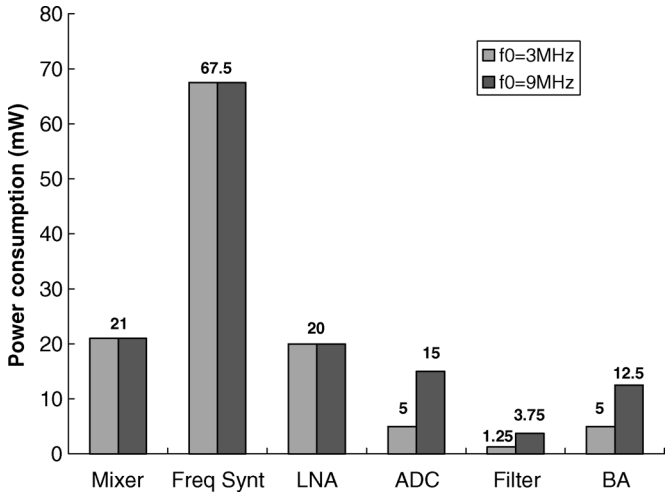

Fig. 14. RF power consumption for different blocks in DCR receiver.

can be moved to a lower IF frequency instead of baseband (see Fig. 13). The base-band amplifier, base-band filter, and ADC now work at a higher frequency and consume more power. The increase in power consumption is especially significant since DVB-H systems have no transmit channel. Therefore, the IF center frequency can be used to establish a tradeoff between RF energy consumption and communication quality.

A. Energy Consumption

From the power models described in Section III, we see that base-band signal center frequency directly affects the power consumption of the base-band amplifier (BA), base-band analog filter, and ADC. Other components are not directly affected by signal frequency. The simulation environment is given in Table IV. Fig. 14 illustrates the phenomenon for two different signal center frequencies: $f_0 = 3$ MHz and $f_0 = 9$ MHz. We see that although the power consumption of BA, ADC, and the base-band analog filter are not very large, the overall power increase in the receiver is about 16.5%, which cannot be ignored in receive-only systems.

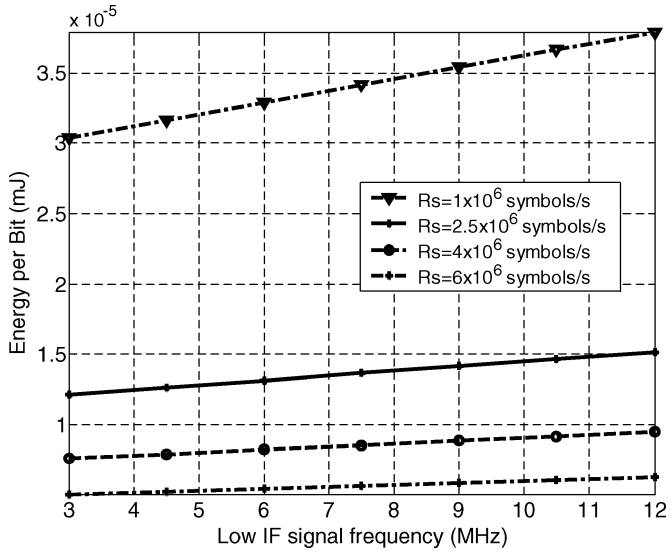

Fig. 15. Receive-only 16 QAM system: Energy consumption per bit for different base-band signal center frequencies.

In the remaining part of this section, we evaluate the energy performance of the system with respect to the active energy per bit, $E_{\rm bit} = (P_{\rm non-freq} + P_{\rm freq})T_{\rm bit}$, where $P_{\rm non-freq}$ represents the sum of the power of the nonfrequency related components and $P_{\rm freq}$ represents frequency related components, respectively. $P_{\rm non-freq}$ is the sum of the power of mixer, frequency synthesizer, and LNA, and is equal to 110 mW according to Table II. In summary

$$E_{\rm bit} = (110 + P_{\rm filter}(f) + P_{\rm BA}(f) + P_{\rm ADC}(f))/(Rsb)$$

where R_s is the symbol rate and b is the number of bits per symbol ($b = log\ M$). Next, we show how the symbol rate R_s, low IF center frequency, and the number of bits per symbol b affect the energy per bit $E_{\rm bit}$.

Fig. 15 shows the effect of the low IF signal center frequency and the symbol rate on the active energy per bit, $E_{\rm bit}$, for 16 QAM ($b = 4$) modulation. For fixed R_s and fixed b (*bits/symbol*), $E_{\rm bit}$ increases with the signal frequency. This is because the base-band analog filter, BA, and ADC work at a higher frequency and consume more power (see Fig. 14). If signal frequency is fixed and $E_{\rm bit}$ is compared for different symbol rates, we can see that as the symbol rate increases, the energy consumption reduces. This is because higher symbol rate results in shorter bit duration ($T_{\rm bit} \propto 1/R_s$). Thus, for 16 QAM modulation, lower IF signal frequency and/or higher symbol rates help reduce $E_{\rm bit}$. Unfortunately, this also deteriorates communication quality as will be shown in the following section. If the symbol rate is low, it is especially important that the signal frequency be kept as low as possible to save energy.

Next, the effect of b, the number of bits per symbol for a fixed symbol rate R_s, and low IF signal frequency is evaluated. Fig. 16 shows that the receiver energy consumption per bit reduces as b

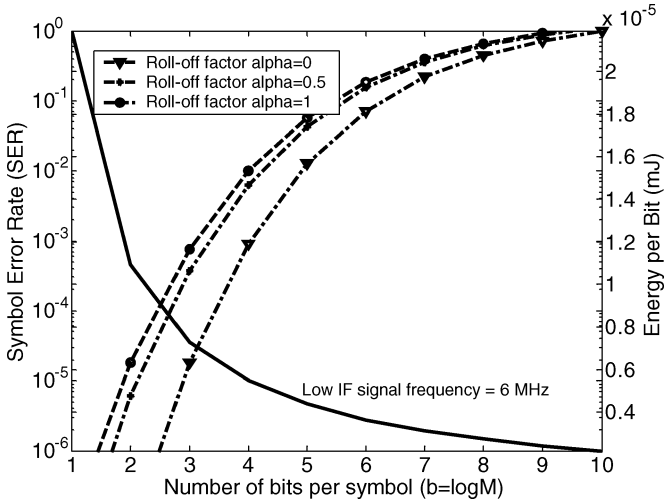

Fig. 16. Receive-only MQAM system: SER and energy per bit versus b.

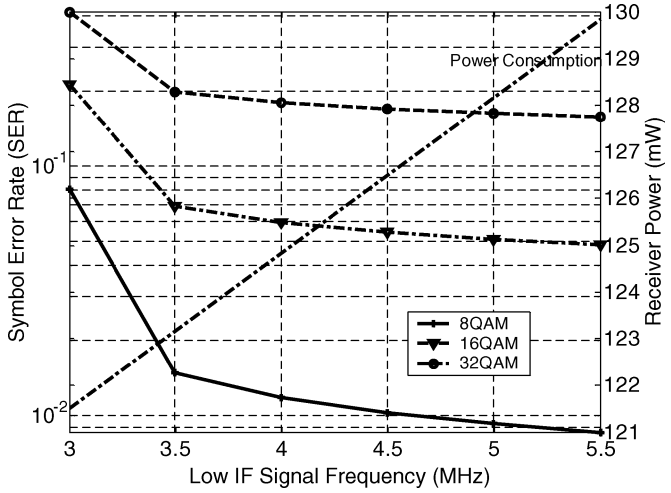

Fig. 17. Receive-only MQAM system: SER and power versus low IF signal frequency; $\alpha = 0.5$.

reduces. This is expected since higher b value results in shorter bit duration ($T_{\text{bit}} \propto 1/b$). Note that the E_{bit} versus b trend for receive-only system is different from that of single user point-to-point communication system (see Fig. 10). This is because there is no PA in the receive-only system, and the effect of increasing PA power with increasing b is nonexistent.

B. Communication Quality

This section describes the effects of low IF signal frequency, roll-off factor α, and b (*bits/symbol*) on the communication quality. If the bandwidth of the bandpass filter in the receiver is the same as that of the signal, the noise power is expressed as shown in (2). If the integrated noise has a Gaussian distribution, then SER can be expressed in a way similar to (23)

$$\text{SER} = 4\left(1-\frac{1}{\sqrt{M}}\right) \cdot Q\left(\sqrt{\frac{3\cdot P_{\text{received}}}{(M-1)\cdot N_0\cdot\left[BW+f_{\text{cor}}\cdot\ln\left(f_0+\frac{BW}{2}\right)/\left(f_0-\frac{BW}{2}\right)\right]}}\right).$$

Assume $\text{SNR}_0 = P_{\text{received}}/(N_0 \cdot BW) = 12$ dB, then SER can be expressed as shown in (26) at the bottom of the page.

Since the pulse shaping filter roll-off factor α changes the signal bandwidth BW by a factor of $(1+\alpha)$ [20] and $M = 2b$, (26) establishes the relation between SER and parameters roll-off factor α, the signal frequency f_0, b (*bits/symbol*).

Fig. 16 also shows how SER increases with the increase in b (*bits/symbol*) for fixed signal frequency and different roll-off factor α. Larger constellation sizes ($M = 2^b$) result in shorter signal distance, making the signal more susceptible to noise. If we fix b (*bits/symbol*) value, smaller α results in better communication quality. This can be explained by the following: the increase in α expands the signal bandwidth and integrates more thermal noise power.

Fig. 17 illustrates how SER reduces with the increase in the signal center frequency for different constellation size ($M = 8$, 16, and 32). If we change the signal frequency from 3 to 5.5 MHz, we find that high signal center frequency reduces the effect of $1/f$ noise.

C. Low Energy System Design for a Specified SER

Figs. 16 and 17 help to design a low energy receive-only system for a given SER specification. There are multiple combinations of low IF signal frequency f_0 and b (*bits/symbol*) that satisfy the SER requirement from Fig. 17. The combination with minimum signal frequency f_0 is chosen, since it leads to minimum energy consumption. Then we utilize Fig. 16 to adjust the roll-off factor α for the best communication quality. Thus, we can determine the combination of roll-off factor α, b (*bits/symbol*), and signal frequency f_0 corresponding to the minimum energy configuration for a given SER.

VII. Conclusion

In this paper, a system level energy model for the RF front-end of a wireless transceiver is developed and the effects of signal bandwidth, PAR, symbol rate, modulation level b (*bits/symbol*), transmission distance, and the signal center frequency on the RF front-end energy consumption and communication quality is considered. Three representative communication systems have been studied: a single user point-to-point system, a CDMA-based multiuser system, and a receive-only system. For single user systems, a detailed study of the effect of PAR on RF energy consumption and SER is presented. It is shown that symbol rate, constellation size, and

$$\text{SER} = 4\left(1-\frac{1}{\sqrt{M}}\right)\cdot Q\left(\sqrt{\frac{3\cdot \text{SNR}_0}{(M-1)\cdot\left[1+\frac{1}{BW}\cdot f_{\text{cor}}\cdot\ln\left(f_0+\frac{BW}{2}\right)/\left(f_0-\frac{BW}{2}\right)\right]}}\right) \tag{26}$$

pulse-shaping roll-off factor can be used to control the energy consumption and communication quality. For multi-user CDMA-based systems, it is shown that the effect of PAR on RF energy consumption is similar to point-to-point single user systems but their effect on SER is different because of MAI. For such systems, the number of users and MAI are also important in deciding the system energy and quality performance. For receive-only systems, the effect of $1/f$ noise and low IF signal center frequency on DVB-H is evaluated. Tradeoffs between the low IF signal center frequency and the energy consumption and communication quality are presented. Future work includes adding the effect of digital power consumption on the energy-quality evaluation.

REFERENCES

[1] C. Schurgers and M. B. Srivastava *et al.*, "Modulation scaling for energy aware communication systems," in *Proc. ISLPED*, 2001, pp. 96–99.

[2] Z. Yang, Y. Yuan, and J. He, "Energy aware data gathering based on adaptive modulation scaling in wireless sensor networks," in *Proc. IEEE VTC*, 2004, pp. 2794–2798.

[3] A. Woo and D. Culler, "A transmission control scheme for media access in sensor networks," in *Proc. 7th Ann. Int. Conf. Mobile Comput. Netw.*, 2001, pp. 221–235.

[4] X. Wang, Y. Ren, and J. Zhao *et al.*, "Energy efficient transmission protocol for UWB WPAN," in *Proc. IEEE VTC2004*, 2004, pp. 5292–5296.

[5] B. Prabhakar, E. U. Biyikoglu, and A. E. Gamal, "Energy efficient transmission over a wireless link via lazy packet scheduling," in *Proc. IEEE INFOCOM*, 2001, pp. 386–394.

[6] R. Ramanathan and R. Rosales-Hain, "Topology control of multihop wireless networks using transmit power adjustment," in *Proc. IEEE INFOCOM*, 2000, pp. 404–413.

[7] D. Li, X. Jia, and H. Liu, "Energy efficient broadcast routing in static ad hoc wireless networks," *IEEE Trans. Mobile Comput.*, vol. 3, no. 2, pp. 144–151, Jun. 2004.

[8] D. Kim, J. Park, and C. K. Toh *et al.*, "Power-aware route maintenance protocol for mobile ad hoc networks," in *Proc. IEEE ICT*, 2003, pp. 501–506.

[9] K. Lahiri, A. Raghunathan, and S. Dey, "Communication based power management," in *Proc. IEEE Design Test Comput.*, 2002, pp. 118–130.

[10] M. Srivatsava, "Power-aware communication systems," in *Power Aware Design Methodologies*. Norwell, MA: Kluwer, 2002.

[11] E. Lauwers and G. Gielen, "Power estimation methods for analog circuits for architecture exploration of integrated systems," *IEEE Trans. Very Large Scale Integr. (VLSI) Syst.*, vol. 10, no. 2, pp. 155–162, Apr. 2002.

[12] P. F. Chen and L. E. Larson *et al.*, "High-efficiency power amplifier using dynamic power-supply voltage for CDMA applications," *IEEE Trans. Microw. Theory Tech.*, vol. 47, no. 8, pp. 1471–1476, Aug. 1999.

[13] C. Wang and L. E. Larson *et al.*, "Improved design technique of a microwave class-E power amplifier with finite switching-on resistance," in *Proc. IEEE RAWCON*, 2002, pp. 241–244.

[14] A. Y. Wang and S. Cho *et al.*, "Energy efficient modulation and MAC for asymmetric RF microsensor system," in *Proc. ISLPED*, 2001, pp. 106–111.

[15] S. Cui and A. Bahai *et al.*, "Modulation optimization under energy constraints," in *Proc. IEEE Int. Conf. Commun. (ICC)*, 2003, pp. 2805–2811.

[16] B. Razavi, *RF Microelectronics*. Englewood Cliffs, NJ: Prentice-Hall, 1998.

[17] X. Li and L. J. Cimini, "Effects of clipping and filtering on the performance of OFDM," *IEEE Commun. Lett.*, vol. 2, no. 5, pp. 131–133, May 1998.

[18] T. A. Wilkinson and A. E. Jones, "Minimization of the peak to mean envelop power ratio in multicarrier transmission schemes by blocking coding," in *Proc. IEEE VTC*, 1999, pp. 825–831.

[19] X. Wang, T. T. Tjhung, and C. S. Ng, "Reduction of peak-to-average power ratio of OFDM system using a companding technique," *IEEE Trans. Broadcast.*, vol. 45, no. 3, pp. 303–307, Sep. 1999.

[20] T. S. Rappaport, *Wireless Communications Principles and Practice*. Englewood Cliffs, NJ: Prentice-Hall, 1996.

[21] M. Gustavsson, J. J. Wikner, and N. N. Tan, *CMOS Data Converters for Communications*. Norwell, MA: Kluwer, 2000.

[22] Y. P. Tsividis, "Integrated continuous-time filter design—an overview," *IEEE J. Solid-State Circuits*, vol. 29, no. 3, pp. 166–176, Mar. 1994.

[23] P. Wambacq, G. Vandersteen, and S. Donnay *et al.*, "Higher-level simulation and power modeling of mixed-signal front-ends for digital communications," in *Proc. IEEE ICECS*, 1999, pp. 525–528.

[24] S. Cui, A. J. Goldsmith, and A. Bahai, "Energy-constrained modulation optimization," *IEEE Trans. Wireless Commun.*, vol. 4, no. 5, pp. 2349–2360, Sep. 2005.

[25] D. Duarte, N. Vijaykrishnan, and M. J. Irwin, "A complete phase-locked loop power consumption model," in *Proc. Design, Autom. Test Eur. Conf. Exhibition (DATE)*, 2002, p. 1108.

[26] C. Schurgers, V. Raghunathan, and M. B. Srivastava, "Power management for energy-aware communication systems," *ACM Trans. Embedded Comput. Syst. (TECS)*, vol. 2, no. 3, pp. 431–447, Aug. 2003.

[27] Y. Le Guillou, O. Gaborieau, and P. Gamand *et al.*, "Highly integrated direct conversion receiver for GSM/GPRS/EDGE with on-chip 84-dB dynamic range continuous-time/spl Sigma//spl Delta/ADC," *IEEE J. Solid-State Circuits*, vol. 40, no. 2, pp. 403–411, Feb. 2005.

[28] C.-H. Heng and B.-S. Song, "A 1.8-GHz CMOS fractional-N frequency synthesizer with randomized multiphase VCO," *IEEE J. Solid State Circuits*, vol. 38, no. 6, pp. 848–854, Jun. 2003.

[29] B. Razavi, "A 1.8-GHz CMOS voltage-controlled oscillator," in *ISSCC Digest Tech. Papers*, 1997, pp. 388–389.

[30] J. Ryynanen, K. Kivekas, and J. Jussila *et al.*, "Dual-band RF front-end for WCDMA and GSM applications," *IEEE J. Solid-State Circuits*, vol. 36, no. 8, pp. 1198–1204, Aug. 2001.

[31] V. Veldhoven and R. H. M. A. , "Triple-mode continuous-time/spl Sigma//spl Delta/modulator with switched-capacitor feedback DAC for a GSM-EDGE/CDMA2000/UMTS receiver," *IEEE J. Solid-State Circuits*, vol. 38, no. 12, pp. 2069–2076, Dec. 2003.

[32] N. Ghittori, A. Vigna, P. Malcovati, and A. Baschirotto, "A low-distortion 1.2 V DAC+filter for transmitters in wireless applications," in *Proc. ISCAS*, 2005, vol. 1, pp. 776–779.

[33] J. Ryynanen, K. Kivekas, and J. Jussila *et al.*, "A single-chip multimode receiver for GSM900, DCS1800, PCS1900, and WCDMA," *IEEE J. Solid-State Circuits*, vol. 38, no. 4, pp. 594–602, Apr. 2003.

[34] H. O. Elwan, M. I. Younus, H. A. Al-Zaher, and M. A. Ismail, "Buffer-based baseband analog front end for CMOS bluetooth receivers," *IEEE Trans. Circuits Syst. II: Analog Digit. Signal Process.*, vol. 49, no. 8, pp. 545–554, Aug. 2002.

[35] Y. C. Yoon, "A simple and accurate method of probability of bit error analysis for asynchronous band-limited DS-CDMA systems," *IEEE Trans. Commun.*, vol. 50, no. 4, pp. 656–663, Apr. 2002.

[36] Y. Asano and Y. Daido *et al.*, "Performance evaluation for band-limited DS-CDMA communication system," in *Proc. IEEE VTC*, 1993, pp. 464–468.

[37] A. J. Viterbi, *CDMA: Principle of Spread Spectrum Communication*. Reading, MA: Addison-Wesley, 1995.

[38] A. A. Abidi, "Low-power radio-frequency IC's for portable communications," *Proc. IEEE*, vol. 83, no. 4, pp. 544–569, Apr. 1995.

[39] A. Georgiadis, "Gain, phase imbalance, and phase noise effects on error vector magnitude," *IEEE Trans. Veh. Technol.*, vol. 53, no. 2, pp. 443–449, Mar. 2004.

[40] B. Sahu and G. A. R. Mora, "A high-efficiency linear RF power amplifier with a power-tracking dynamically adaptive buck-boost supply," *IEEE Trans. Microw. Theory Tech.*, vol. 52, no. 1, pp. 112–120, Jan. 2004.

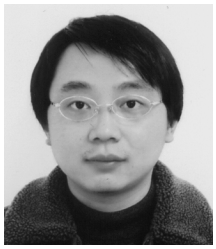

Ye Li received the B.S. and M.S. degrees in electrical engineering from University of Electronic Science and Technology of China (UESTC), Chengdu, China, in 1999 and 2002, respectively, and the Ph.D. degree in electrical engineering from Arizona State University (ASU), Tempe, in 2006. His Ph.D. thesis was on low power wireless communication and wireless multimedia system design.

His research interests include low power RF transceiver design, global optimization for wireless communication system, and wireless video system.

Bertan Bakkaloglu (M'94) received the Ph.D. from Oregon State University, Corvallis, in 1995.

He was with Texas Instruments Inc. Mixes Signal Wireless Design Group, Dallas, TX, where he is working on analog, RF, and mixed signal front ends for wireless and wireline communication ICs. He worked on system-on-chip designs with integrated battery management and analog baseband functionality as a Design Leader. In 2001, he joined the Broadband Communications Group where he worked on cable modem analog front-end designs and Gigabit Ethernet front-ends. In 2004, he joined Arizona State University, Electrical Engineering Department, Tempe, as an Associate Professor. His research interests include RF and PA supply regulators, RF synthesizers, high speed RF data converters, and RF built-in-self-test circuits for communication ICs. He holds three patents. He has been a technical program chair for ISCAS and MTT/RFIC conferences and Associate Editor for the IEEE TRANSACTIONS ON CIRCUITS AND SYSTEMS.

Chaitali Chakrabarti (SM'02) received the B.Tech. degree in electronics and electrical communication engineering from the Indian Institute of Technology, Kharagpur, India, in 1984, and the M.S. and Ph.D. degrees in electrical engineering from the University of Maryland, College Park, in 1986 and 1990, respectively.

Since August 1990, she has been with the Department of Electrical Engineering, Arizona State University (ASU), Tempe, where she is now a Professor. Her research interests include the areas of low power embedded systems design including memory optimization, high level synthesis and compilation, and VLSI architectures and algorithms for signal processing, image processing, and communications.

Dr. Chakrabarti is a member of the Center for Low Power Electronics, the Consortium for Embedded Systems, and Connection One. She is a recipient of the Research Initiation Award from the National Science Foundation in 1993, a Best Teacher Award from the College of Engineering and Applied Sciences from ASU in 1994, and the Outstanding Educator Award from the IEEE Phoenix Section in 2001. She has served on the program committees of ICASSP, ISCAS, SIPS, HPCA, ISLPED, and DAC. She is an Associate Editor of the *Journal of VLSI Signal Processing Systems* and served as an Associate Editor of the IEEE TRANSACTIONS ON SIGNAL PROCESSING (1999–2004). She is currently the TC Chair of the sub-committee on Design and Implementation of Signal Processing Systems, IEEE Signal Processing Society.